Research Article

Zn_2TiO_4 photoluminescence enhanced by the addition of Cr^{3+}

Sandra da Silva Pedro[1] · **Ada López**[1] · **Lilian Pantoja Sosman**[1]

Received: 4 October 2019 / Accepted: 5 December 2019 / Published online: 7 December 2019

Abstract
In this work, the photoluminescent properties of Zn_2TiO_4:Cr^{3+} are presented. Samples were prepared from ZnO, TiO_2 and Cr_2O_3 by solid-state reaction. The compound formation was confirmed by X-ray diffraction. Emissions were obtained using photoluminescence spectroscopy at room temperature. The system crystallizes in the space group $Fd\bar{3}m$ with an inverse spinel structure. The emission spectrum presents a broad and intense band in the near-infrared region. Photoluminescence excitation shows two bands in the visible frequency range assigned to octahedral Cr^{3+} transitions. Cr^{3+}-doped and undoped sample emissions were compared. Optical spectra were analyzed and interpreted according to the crystal field theory and the Tanabe–Sugano energy matrices for the d^3 configuration by calculating the Dq and B parameters. This work is a follow-up of the previous research on transition metal cations used as dopants in a Zn_2TiO_4 lattice, and the current results suggest that the system might be a promising luminescence source at room temperature.

Keywords Photoluminescence · Optical ceramics · Transition metal doping

1 Introduction

Several physical properties of zinc orthotitanate (Zn_2TiO_4) have been exhaustively investigated, including dielectric features, especially in the microwave range [1, 2], semiconductor characteristics [3] and photocatalytic properties [4], among others. The versatility of the compound allows its use as a catalytic sorbent for the removal of contaminants from hot coal gases and in the chemical industry [1], in white color pigmentation [5], as a sensor component [6] or an inorganic antimicrobial agent [7], and even in forensic applications [8]. The synthesis might be performed through a conventional solid-state reaction between ZnO and TiO_2 in a 2:1 ratio, but other methods are also used [9].

The crystal structure of Zn_2TiO_4 has been reported as cubic in an inverse spinel of the B[AB]O_4 type, where the letters in the brackets enclose the octahedrally coordinated atoms. The zinc orthotitanate crystal structure is represented by Zn[ZnTi]O_4, meaning that Zn and Ti are randomly found at the octahedral sites, while the tetrahedral sites are fully occupied by Zn [10]. A detailed graphic structure representation can be seen in [7]. In this way, it is possible to find Zn^{2+} cations in both octahedral and tetrahedral coordinations, while the Ti^{4+} cations are only found in the octahedral environment. These structural features make Zn_2TiO_4 an interesting material for optical spectroscopy studies since this compound has both octahedral and tetrahedral sites available for occupation by potential dopants.

Concerning the optical properties, the luminescence of a transition metal acting as a dopant in a crystal might occur in the visible and/or near-infrared regions of the electromagnetic spectrum. The emission energy position depends on the electronic configuration of the dopant cation, according to the Tanabe–Sugano diagrams for d^2–d^8 electronic configurations [11–13]. In configurations where the excited level energy decreases as the crystal field parameter Dq increases, the emission is likely to occur in the red/near-infrared region if the dopant cation is found in an octahedral environment, while an emission can occur

✉ Sandra da Silva Pedro, sandrapedro@uerj.br | [1]Instituto de Física Armando Dias Tavares, Universidade do Estado do Rio de Janeiro, Rio de Janeiro, RJ 20550-900, Brazil.

in the visible region if the dopant is at a tetrahedral site. On the other hand, if the level increases in energy as *Dq* increases, the transition might be in the visible or near-infrared region if the cation is at an octahedral site and in the infrared region if the dopant is in tetrahedral symmetry. For states that are independent of the crystal field parameter *Dq*, the energy position of the transition will not change, regardless of whether the cation is at a tetrahedral or an octahedral site. For spectroscopic properties, this feature opens the possibility of obtaining emissions in a broad range of wavelengths, allowing the generation of tunable bands, depending on the electronic configuration of the dopant and its position in the host lattice.

Several works report the photoluminescent properties of the zinc titanates both undoped and doped with transition metal and rare earth cations, confirming the versatility of the compound in terms of optical properties and its semiconductor character. Markevich mentions the photoluminescence of the undoped Zn_2TiO_4 compound with a band at 720 nm [14]. Chaves presented the photoluminescence of a Zn_2TiO_4 powder doped with Sn^{4+}, V^{5+} and Cr^{3+}, showing that the emission increases when the dopants are added to the lattice, associating this behavior with a short-range disorder [9]. Previous works developed by our research group studied the photoluminescent properties of this compound doped with transition metal cations. Sosman describes the emission properties of Zn_2TiO_4:Mn^{2+}, showing bands in the green (532 nm) and red (690 nm) wavelengths assigned to the spin-forbidden transitions of Mn^{2+} with dopant occupation at tetrahedral and octahedral sites, respectively [15]. Espinoza details the emission of this system doped with Co^{2+} related to a broadband in the infrared region at 714 nm assigned to the occupation of Co^{2+} at the tetrahedral sites, replacing Zn^{2+} [16]. A work reporting the optical properties of this lattice doped with Ni^{2+} is in development and will be published soon. Lokesh presents the optical properties of $Zn_{1-x}Cu_xTiO_3$, showing that the addition of Cu enhanced the photoluminescence of the undoped lattice in the UV region [17]. Girish investigated Zn_2TiO_4:Eu^{3+}, Zn_2TiO_4:Dy^{3+} and Zn_2TiO_4:Sm^{3+} and found that the narrow band emission of these phosphors in the visible region is related to the f–f transitions of rare earth dopants [6, 8, 18].

In this study, we give a follow-up of our previous research [15, 16], presenting the synthesis by solid-state reaction of Zn_2TiO_4 doped with Cr^{3+}, investigating the formation of the compound by X-ray diffraction measurements and using Rietveld refinement. Photoluminescence (PL), photoluminescence excitation (PLE) and emission decay measurements were used to determine the spectroscopic properties of the synthesized compound, and the emissions of the doped and undoped samples were compared. Optical spectra were analyzed and interpreted according to the crystal field theory and the Tanabe–Sugano energy matrices for the d^3 configuration by calculating of the crystal field *Dq* and Racah *B* parameters. This paper presents the results of a study to obtain an optical system with a simple and inexpensive preparation that has the potential for the creation of a material that could operate in a wide emission range at room temperature.

2 Materials and methods

Samples were synthesized with the conventional solid-state reaction using zinc (ZnO), titanium (TiO_2) and chromium (Cr_2O_3) oxides in powder form with a high purity level (> 99.9%) as the reagents, weighed according to the stoichiometric reaction presented in Eq. 1 (where $x = 0.001$).

$$2\left(1-\frac{x}{2}\right)ZnO + TiO_2 + \frac{x}{2}Cr_2O_3 \rightarrow Zn_{2-x}Cr_xTiO_4 + \frac{x}{2}O_2 \quad (1)$$

Powder oxides were manually crushed with an agate mortar and pestle to homogenize the powder. Subsequently, the powder was compacted into pellets with 13 mm diameter and 1 mm thickness under a pressure of 4 t. The pellets were deposited in alumina crucibles and underwent thermal treatment at 1200 °C for 10 h with a furnace heating rate of 10 °C/min in an electric furnace under atmospheric pressure. At the end of the thermal synthesis, the furnace was switched off and left to cool down to room temperature by thermal inertia. Samples exhibited a homogeneous light green color, indicating that Cr^{3+} was incorporated into the host lattice. The pellets were removed from the furnace at room temperature, and one pellet was reground until a homogeneous, thin powder was obtained for X-ray diffraction.

The powder X-ray diffraction pattern was obtained at room temperature using a *Bruker* D2 Phaser diffractometer with Cu-Kα_1 radiation ($\lambda = 1.54056$ Å) operating at 30 kV and 10 mA. Data were collected in a Bragg–Brentano geometry with $15° < 2\theta < 65°$ and a step size of 0.01°. X-ray diffraction data were refined using the Rietveld method with the *Fullprof* package [19]. Rietveld refinement provides information about the space group, lattice parameters and phase quantification. The observed data were compared to those from files extracted from the ICSD (Inorganic Crystal Structure Database).

Photoluminescence experiments (emissions, excitation spectra and emission decay) were performed at room temperature using a *PTI 300 QuantaMaster* spectrofluorometer equipped with a 75 W pulsed xenon lamp operating at 200 Hz and variable spectral resolution. Filters were used to block excitation wavelengths in the detection

apparatus. All optical spectra were corrected by the apparatus sensitivity response.

3 Results and discussion

3.1 Crystal structure

Figure 1 shows the sample powder diffractogram recorded at room temperature. The most intense peaks were assigned to the zinc orthotitanate phase, and a few peaks of lower intensity were assigned to unreacted zinc oxide (ZnO). Rietveld refinement was performed using experimental data together with cubic Zn_2TiO_4 (ICSD code 80851) and hexagonal ZnO (ICSD code 067849) data as input. Agreement factors and the difference between the calculated and observed profiles were evaluated at each refinement cycle to determine the refinement quality. The agreement factors presented in Table 1 point to a good correspondence between the refined and observed patterns. The goodness-of-fit factor (GOF) extracted from the refinement was 1.6, indicating good refinement quality.

According to the refinement analysis, the phase proportion is approximately 98% for the main phase (Zn_2TiO_4) and nearly 2% for ZnO, the latter likely being a small, unreacted quantity in the synthesis process. The main compound crystallizes in the $Fd\bar{3}m$ space group, with cubic symmetry and lattice parameter $a = 8.469(9)$ Å. Additional details of the Rietveld refinement are given in Table 1. The

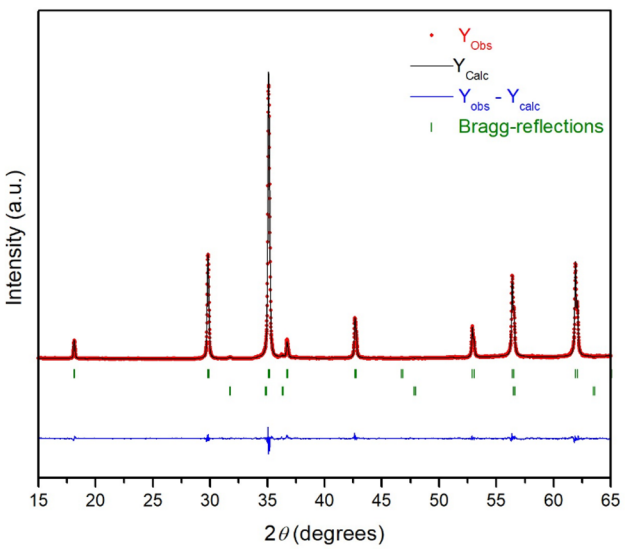

Fig. 1 Powder X-ray diffractogram of the sample. The red circles represent the observed pattern (Y_{obs}), the black line represents the calculated pattern (Y_{calc}) and the blue line is the difference between the calculated and observed patterns ($Y_{obs} - Y_{calc}$). The green vertical bars represent the Bragg reflections of the Zn_2TiO_4 (top) and ZnO (bottom) phases

Table 1 Refined crystallographic parameters and agreement factors

Phase	Zn_2TiO_4	ZnO
ICSD code	80851	067849
Proportion (%)	98.01	1.99
Crystal system	Cubic	Hexagonal
Space group	$Fd\bar{3}m$	$P6_3mc$
a, *b*, *c* (Å)	8.469(9), 8.469(9), 8.469(9)	3.255(6), 3.255(6), 5.142(4)
α, *β*, *γ* (°)	90, 90, 90	90, 90, 120
Cell volume (Å^3)	607.43	47.20

Agreement factors: $R_{wp} = 9.52$, $R_p = 9.61$, $R_{exp} = 5.78$, $\chi^2 = 2.70$, GOF = 1.60

Zn_2TiO_4 crystal structure is described as an inverse spinel, where the Zn^{2+} cations are found at octahedral and tetrahedral sites, while the Ti^{4+} cations are found only in the octahedral environment, as previously mentioned [10, 20].

The percentage difference between the atomic radii of the inserted and replaced atoms must be less than 30% according to Girish and coauthors [6]. In the present case, the atomic radius of Zn^{2+} is 0.60 Å when its coordination number (CN) is 4 and 0.74 Å for CN = 6; for Ti^{4+}, this value is 0.61 Å; and for Cr^{3+}, it is 0.62 Å, both for CN = 6 [21]. Comparing all numbers, it is possible to say that Cr^{3+} can replace both the Zn^{2+} and Ti^{4+} cations in octahedral and tetrahedral symmetries. Furthermore, the distinct valences of the dopant and the replaced cations (+2 for Zn, +4 for Ti and +3 for Cr) may lead to a charge compensation process, which is believed to be more favorable for the replacement of Zn^{2+} by Cr^{3+} because this replacement requires an electron to compensate the charge; this electron might be shared from the O^{2-} anions, which may generate a covalent bond between the Cr^{3+} cations and the O^{2-} anions.

Another question is related to the occupation possibility of Cr^{3+} at the ZnO sites. The ZnO crystal structure is hexagonal and belongs to the space group $P6_3mc$, where the Zn^{2+} cations are tetrahedrally coordinated by the O^{2-} anions. Two observations lead us to believe that Cr^{3+} does not occupy the ZnO sites: First, the mass quantity of ZnO is small when compared to the main phase, leading to a very low probability of Cr^{3+} occupation of the ZnO sites, as the Cr^{3+} doping concentration is also very small; second, it is well known that Cr^{3+} tends to preferentially occupy octahedral instead of tetrahedral sites in a structure with both environments. Although neither the cations and dopant valences nor the ionic radii values point to a direct identification of Cr^{3+} occupation in this structure, optical measurements may indicate the type of symmetry that this cation occupies, according to the position and shape of the observed emission and excitation bands.

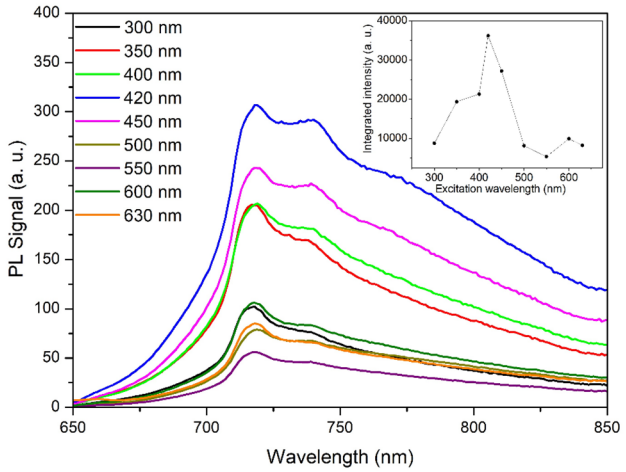

Fig. 2 Cr^{3+}-doped zinc orthotitanate photoluminescence (PL) spectra excited with several wavelengths at room temperature. Structures were observed at 719 and 740 nm. Inset: dependence of the bands' integrated intensity with the excitation wavelength

3.2 Photoluminescent properties

Figure 2 exhibits the photoluminescence spectra of the chromium-doped zinc orthotitanate for several excitation wavelengths in the 300–630 nm range at room temperature. All spectra exhibit a broadband with structures at 719 nm (13908 cm^{-1}) and 740 nm (13531 cm^{-1}). The integrated intensity as a function of the excitation wavelength is shown in the inset in Fig. 2. It is possible to observe that the emission signal increases with UV and blue excitation with the signal maximized at 420 nm and decreases as the excitation wavelength increases. The excitation wavelengths that are more favorable for emission are found in the 400–450 nm range. Several factors can be considered for the dramatic decrease in the emission intensity: the low probability of incident external radiation absorption, competition of nonradiative processes, or temperature or dopant concentration effects. In the present case, the hypothesis is that the emission intensity reduction starting at 450 nm can be explained by the occurrence of nonradiative processes that must be more effective than for 420 nm wavelength.

In addition, the shape and band structures do not change significantly with distinct excitation wavelengths in this range; they change only in intensity. Such behavior may indicate the absence of impurity occupation of sites with distinct symmetries.

It is well known that trivalent chromium exhibits a broad emission band in the near-infrared region when the cation occupies octahedral sites in ceramic hosts [22, 23], which could lead us to conclude that the observed band could be attributed solely to Cr^{3+} emission. However, previous works in the literature mention that the zinc orthotitanate lattice has an emission band in the same region of the band observed in the present work. Sosman [15] and Markevich [14] reported that undoped Zn_2TiO_4 exhibits a broadband emission in the 600–800 nm range with maxima at 717 and 720 nm, respectively. To verify whether the lattice exhibits such an emission signal, an undoped sample was produced using the same experimental conditions mentioned in the experimental section [but with $x = 0$ in Eq. (1)], and its emission spectrum was recorded with an excitation wavelength of 420 nm. The structure formation was confirmed by X-ray diffraction and investigated in a previous work [15]. The undoped zinc orthotitanate emission spectrum is shown in Fig. 3. The same figure shows the spectrum of the Cr^{3+}-doped sample, which was also excited at 420 nm. The observed emission spectrum of the undoped sample is a broadband with a maximum at 718 nm. The origin of the undoped sample emission is probably related to defects in the inverse spinel structure originated by cationic disorder [24]. Comparing the intensity of the undoped and doped spectra, the doped spectrum exhibits a very broad and intense band, while the undoped spectrum exhibits a weak band. (In fact, Fig. 3 shows that the undoped spectrum was multiplied by 65 to compare it with the doped spectrum.)

Chaves and coauthors previously reported the synthesis by polymeric precursor method and emission of Zn_2TiO_4:Cr^{3+}, as previously mentioned [9]. However, in that paper, the emission intensity of the doped sample did not significantly increase as observed in the present paper. Chaves reported that the maximum intensity of the most intense emission among the doped samples was five times

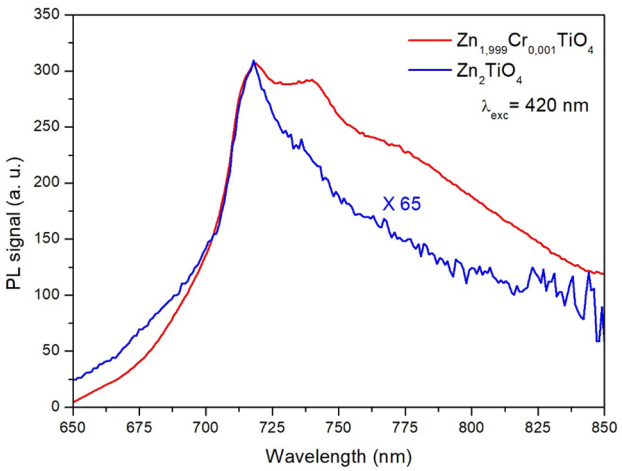

Fig. 3 Photoluminescence spectra obtained at room temperature with an excitation wavelength of 420 nm for the undoped (blue line) and Cr^{3+}-doped (red line) Zn_2TiO_4 samples. For comparison, the undoped sample spectrum was multiplied by 65

more intense than that of the undoped sample. On the other hand, the doped sample emission presented in this work is 65 times more intense than the undoped emission, as shown in Fig. 2. In addition, the emission of our samples is in a distinct spectral region that was observed in [9], but the emission of the undoped samples agrees with [14].

Analyzing the spectra exhibited in Fig. 3, it is first noted that the band format has been slightly changed from the undoped to the doped sample, and the intensity has been dramatically increased with the insertion of Cr^{3+}. If the emission signal had increased in intensity and the band shape had dramatically changed to the point of "erasing" the undoped sample emission memory, we would be able to say that the insertion of Cr^{3+} caused the extinction of the lattice emission, with all absorbed radiation being transferred to the Cr^{3+} emitting state. However, the band shape of the doped sample was not changed dramatically when compared with the undoped sample, preserving the "memory" of the undoped sample emission. In this way, in the spectrum of the doped sample, there is still a contribution from the crystal lattice. As the emission intensity increased as a whole, most likely some of the energy absorbed by Cr^{3+} was transferred to the lattice and intensified its emission.

The Cr^{3+} ion has the electronic configuration [Ar]-$3d^3$, having three unpaired electrons in the 3*d* sublevel. As the sublevel *d* is incomplete, with its electrons in an outer shell, this shell is strongly affected by the electrostatic potential (crystal field) produced by the oxygen anions of the Zn_2TiO_4 crystal lattice. The emission bands are generated by electronic transitions assisted by vibrational modes between the energy levels of the transition metal cation. The shift in energy states depends on the intensity of the crystal field, which is proportional to $< r^4 >$ (the average value of the dopant ionic radius) and a^{-5} (where *a* is the ion–ligand distance) [25]. The interelectronic repulsion, which defines the covalent or ionic character of the ligand–impurity bond, also plays an important role in the shift of the energy states [25].

In this way, we can assign the broadband in the emission spectrum (Figs. 2 and 3) to the $^4T_2(^4F) \rightarrow {}^4A_2(^4F)$ spin-allowed transition of Cr^{3+}, with this emission strongly overlapping with the host emission peak at 719 nm. This emission is typical of Cr^{3+} in octahedral symmetry. This assignment considers the overlap between the dopant and the lattice emissions.

The excitation spectra of the undoped and doped samples are depicted in Fig. 4a. The PLE spectrum for the undoped sample monitored at 718 nm has a very low intensity when compared with the doped spectrum monitored at 740 nm. The weak intensity of the PLE spectrum of the undoped sample agrees with its respective PL spectrum (Fig. 3), where it is observed that the emission of the undoped sample is also weaker than that of the doped sample. Figure 4b depicts the same photoluminescence excitation (PLE) spectrum for the doped sample with its emission monitored at 740 nm shown in Fig. 4a, accompanied by the Gaussian fit of the bands. The two bands in the visible region present features related to the electronic transitions of d^3 ions inserted at the octahedral sites. The bands' barycenter was obtained by Gaussian fitting of the spectrum. The bands

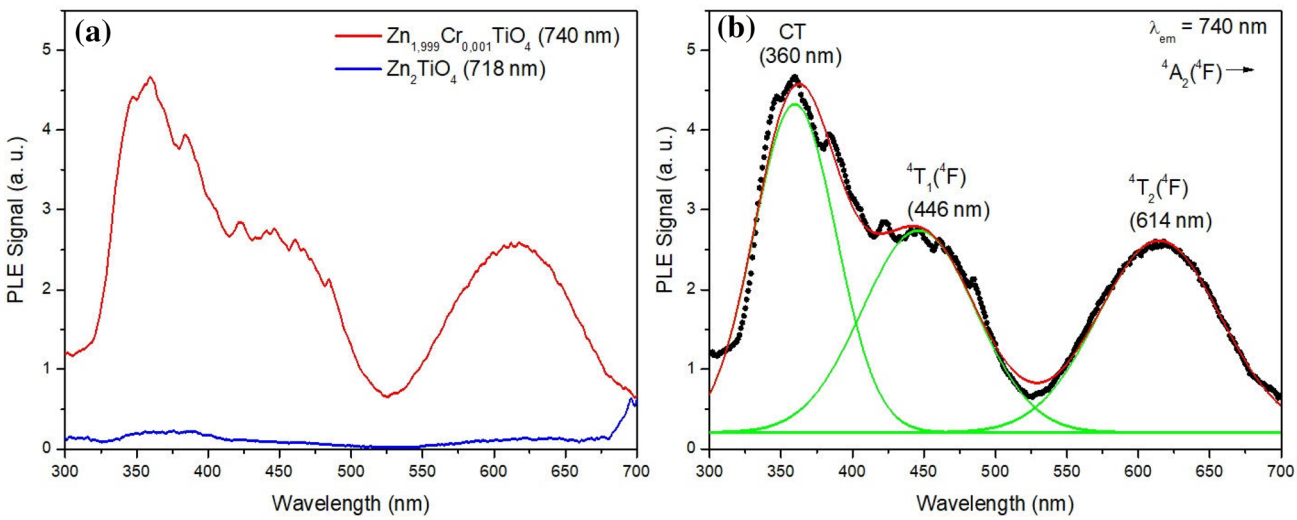

Fig. 4 **a** PLE spectrum for the undoped (blue) and Cr^{3+}-doped (red) samples, monitored at 718 nm and 740 nm, respectively. **b** PLE spectrum (black points) monitored at 740 nm for the Cr^{3+}-doped sample. Three bands were identified: The band at 360 nm is assigned to the charge transfer (CT) processes, and the remaining two are assigned to the Cr^{3+} transitions at the octahedral sites. The adjusted bands (green solid lines) were obtained from a Gaussian fitting (red solid line) from the experimental data

with barycenters at 446 nm (22421 cm^{-1}) and 614 nm (16287 cm^{-1}) were assigned to the $^4A_2(^4F) \rightarrow {}^4T_1(^4F)$ and $^4A_2(^4F) \rightarrow {}^4T_2(^4F)$ trivalent chromium electronic transitions, respectively. The band shape is another indication that Cr^{3+} is inserted in the octahedral environment in the zinc orthotitanate lattice. An intense band with a barycenter at 360 nm (27778 cm^{-1}) was found to be superimposed on the Cr^{3+} higher energy band. This intense band in the UV region is probably related to the Zn–O charge transfer band [8]. As shown in the excitation spectrum in Fig. 4, the doped sample exhibits considerable photoluminescence excitation in the regions below 500 nm and above 550 nm. The low-PLE region (500–550 nm) corresponds to the green light, which justifies the color of the sample observed with the naked eye as previously mentioned in the experimental section, indicating that the sample reflects green light and is better excited by the other wavelengths.

According to the Tanabe–Sugano theory [11–13], it is possible to predict the electronic transitions observed in systems doped with transition metals with incomplete *d* shell and to determine the intensity of the crystal field parameter *Dq* from the energies of these transitions. For d^3 cations in octahedral symmetry, the ground level is $^4A_2(^4F)$. For systems with intense crystal field, the first excited state is $^2E(^2G)$; for weak crystal field, the first excited state is $^4T_2(^4F)$. The Dq/B ratio $\simeq 2.3$ separates high- ($Dq/B > 2.3$) from low- ($Dq/B < 2.3$) crystal field systems, where *B* is one of the Racah parameters. From the Tanabe–Sugano matrices for d^3 systems [11–13, 25] and using the energy values of the identified transitions in the PLE spectrum, it is possible to determine the value of the crystal field *Dq* and the Racah parameter *B*. The calculated values were $Dq = 1629\ cm^{-1}$ and $B = 615\ cm^{-1}$, with $Dq/B = 2.65$. It is important to note that although the $^4T_2(^4F)$ band was undoubtedly identified, the $^4T_1(^4F)$ band was only obtained from a graphical fitting, and its position was only estimated (the CT band is strongly overlapped with this band, as shown in Fig. 4). For this reason, the *B* value might contain an uncertainty greater than that of the *Dq* value. The $^2E(^2G) \rightarrow {}^4A_2(^4F)$ transition was not observed in the emission or excitation spectra, because such an emission generates a spin-forbidden band that was probably hidden by the intense and broadband emission originated at room temperature from the spin-allowed $^4T_2(^4F) \rightarrow {}^4A_2(^4F)$ electronic transition. The value of the Racah parameter *B* is lower than the free ion value ($B_0 = 918\ cm^{-1}$ [26]), as expected. In addition, the ratio $B/B_0 = 0.67$ indicates a strong covalent trend in the Cr^{3+}–O^{2-} bond. This result corroborates our hypothesis that a strong covalent bond between Cr^{3+} and O^{2-} might be used as a charge compensation mechanism due to the Cr^{3+} doping if this cation replaces Zn^{2+} cations in the crystal lattice.

The Cr^{3+} electrons are promoted to the $^4T_1(^4F)$ excited state by light absorption, and they decay via a nonradiative process to the $^4T_2(^4F)$ state, losing this energy to the lattice (Fig. 5a) and resulting in a Stokes shift of $\Delta S = 2756\ cm^{-1}$. This value of the Stokes shift is large enough to observe that the overlap of the emission and excitation bands is small. From the $^4T_2(^4F)$ state, the electrons decay to the ground state, and the system emits luminescence (Fig. 5b).

It is possible to observe from the excitation spectrum of the undoped sample (Fig. 4a) that there are two weak bands in the same regions of the excitation spectrum of the doped sample. This means that if the undoped sample absorbs some radiation in one of these two ranges, then this excitation is able (albeit weakly) to generate luminescence. That said, if Cr^{3+} absorbs energy and transfers a part of it to the lattice, that transferred energy will be added to the energy directly absorbed by the lattice, leading to an intensification of the lattice emission. In addition, the energy absorbed by Cr^{3+} that is not transferred to the lattice will also result in cation emission. The Cr^{3+} emitting state populates the lattice emitting state, intensifying this emission. In this way, the emission band of the doped sample has a shape that reflects the lattice + Cr^{3+} emission overlap.

In an intermediate crystal field system (as in the Cr^{3+} case), the ion interaction with its neighbors is more effective. This makes the doping ion more likely to be

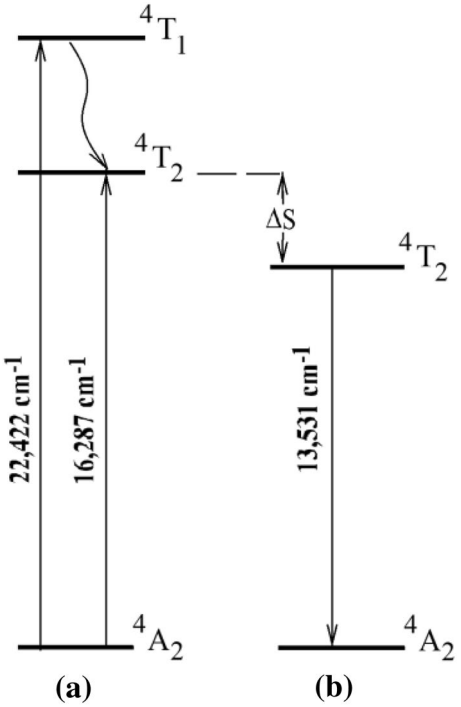

Fig. 5 Cr^{3+} energy level diagram showing the energy levels related to the excitation (**a**) and emission (**b**) bands. Δ*S* is the Stokes shift

influenced by molecular and ligand vibrations. In other words, the dopant energy states are strongly influenced by the lattice phonons. The closer the excitation radiation approaches the red/near-infrared range, the more the vibrational modes (phonons) are excited. Lattice phonons, while helping in the electronic–vibrational transitions of transition metal ion-doped crystal systems, are also responsible for decreasing and even extinguishing the luminescence if a certain limit is exceeded. This limit will depend on the system studied. For the investigated sample, this mechanism is likely responsible for the lower intensity in the emission bands excited with wavelengths over 420 nm when compared to the emission obtained when excited with 420 nm.

3.3 Time decay measurements

Figure 6 exhibits the emission decay curves recorded using 420 nm as the excitation wavelength monitored at (a) 719 nm and (b) 740 nm. Both decay curves exhibit an exponential profile, and the data were fitted with a biexponential function

$$I(t) = A_1 e^{-t/\tau_1} + A_2 e^{-t/\tau_2} \quad (2)$$

where $I(t)$ is the emission intensity at an arbitrary time t, A_1 and A_2 are constants and τ_1 and τ_2 are the decay times for each component [8, 27].

The values for each parameter obtained from the fitting are given in Table 2. A slow and fast decay part is observed in the decay constants. The fast decay (short decay time) is associated with spin-allowed transitions and the slow decay (long decay time) with spin-forbidden transitions. In the case of the octahedral Cr^{3+} cations, the decays from the $^4T_2(^4F)$ state are on the order of microseconds, while those from the $^2E(^2G)$ state are on the order of milliseconds. As the excitation results indicate that the Cr^{3+} cation is in the crystal field close to the $^4T_2(^4F)$ and $^2E(^2G)$ level crossing region, the emission band supposedly contains components from these two states, which explains the lifetimes composed of two exponential parts (slow and fast).

Table 2 Fitting parameters and lifetimes extracted from the biexponential fitting of the radiative decay curves

Emission	A_1	A_2	τ_1 (μs)	τ_2 (μs)
719 nm	91 (2)	46 (2)	159 (3)	588 (24)
740 nm	70 (2)	124 (1)	395 (4)	94 (1)

4 Conclusions

In this work, the synthesis, crystal structure analysis and photoluminescent properties of Cr^{3+}-doped zinc orthotitanate are presented. This work is a follow-up of the previous research on transition metal cations used as dopants in a Zn_2TiO_4 lattice. X-ray diffraction confirmed zinc orthotitanate as the main phase accompanied by a small quantity of unreacted zinc oxide. Photoluminescence experiments at room temperature were performed, and their results were interpreted using the Tanabe–Sugano (TS) theory. Emission and excitation bands confirmed that Cr^{3+} was incorporated at octahedral sites, and the impurity intensified the lattice emission, with the lattice and impurity emissions superimposed. Photoluminescence data did not show evidence of Cr^{3+} at the tetrahedral sites in the energy interval investigated. The Racah B parameter value points

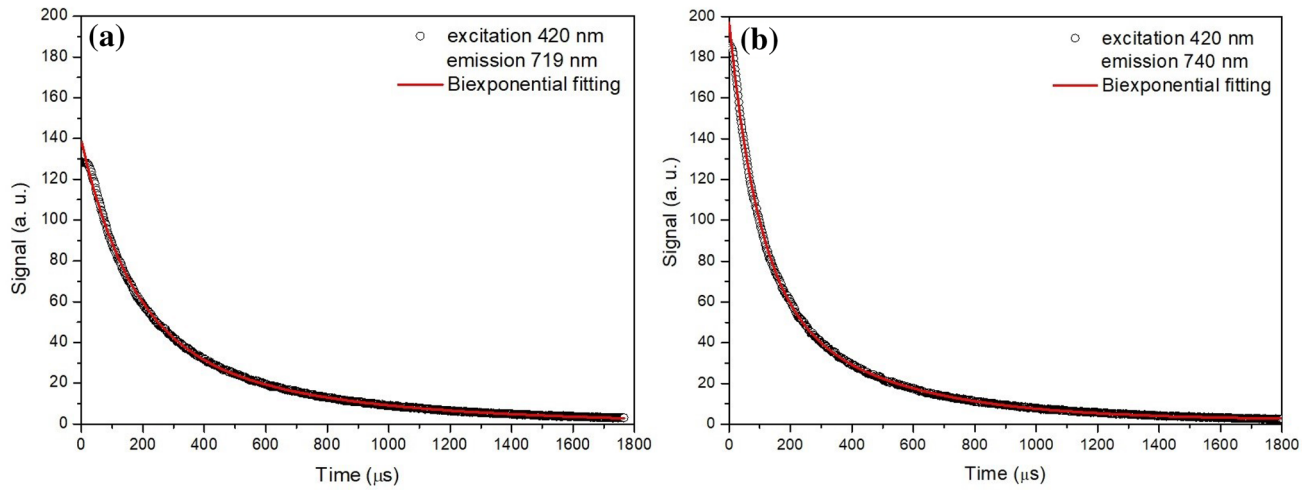

Fig. 6 Photoluminescence decay curves of the doped sample excited at 420 nm with emissions monitored at **a** 719 nm and **b** 740 nm. Open circles are the experimental data, and the red solid curves are the fits obtained from biexponential functions

to a replacement of Zn^{2+} by Cr^{3+} since its value corroborates a strong covalent bond, which also indicates a possible charge compensation mechanism due to the distinct valences between the dopant and the replaced cation. To our knowledge, this is the first time that the energy levels and parameters of Cr^{3+} have been investigated in the Zn_2TiO_4 lattice. The intense and broad emission band in the near-infrared region intensified by the presence of the dopant makes this a system with the potential for use in tunable devices operating in the near-infrared region.

Acknowledgements This study was financed in part by the Coordenação de Aperfeiçoamento de Pessoal de Nível Superior - Brasil (CAPES) - Finance Code 001. The authors are also grateful to the Fundação Carlos Chagas Filho de Amparo à Pesquisa do Estado do Rio de Janeiro (FAPERJ) for their financial support. The authors also thank LIETA-UERJ, Brazil for the X-ray diffraction measurements. L. P. Sosman and S. S. Pedro thank the Conselho Nacional de Desenvolvimento Científico e Tecnológico - CNPq for their Research Productivity fellowships. S. S. Pedro gives thanks for the Jovem Cientista do Nosso Estado (JCNE-FAPERJ) fellowship.

Compliance with ethical standards

Conflict of interest The authors declare no conflict of interest.

References

1. Li L, Li F, Cui T, Zhou Q, Xu D (2012) Optical interband transitions in Zn_2TiO_4 single crystals. Phys Stat Solidi A 12:2596–2599
2. Kim HT, Byun JD, Kim Y (1998) Microstructure and microwave dielectric properties of modified zinc titanates (II). Mater Res Bull 33:975–986
3. Yoon KH, Cho J, Kang DH (1999) Physical and photoelectrochemical properties of the TiO_2–ZnO system. Mater Res Bull 34:1451–1461
4. Borse PH, Cho CR, Lim KT, Lee YJ, Bae JS, Jeong ED, Kim HG (2011) Ratio dependence of the visible light photocatalytic efficiency for $Zn_2Ti_{09}Cr_yFe_{[01-y]}O_4$:Cr/Fe (0002 < y<008) photocatalyst synthesized by using a solid state reaction method. J Korean Phys Soc 59:65–70
5. Ayed S, Abdelkefi H, Khemakhem H, Khemakhem H, Matoussi A (2016) Solid state synthesis and structural characterization of zinc titanates. J Alloy Compd 677:185–189
6. Girish KM, Naik R, Prashantha SC, Nagabhushana H, Nagaswarupa HP, Anantha Raju KS, Premkumar HB, Sharma SC, Nagabhushana BM (2015) Zn_2TiO_4:Eu^{3+} nanophospor: self explosive route and its near UV excited photoluminescence properties for WLEDs. Spectrochim Acta A 138:857–865
7. Perfler L, Kahlenberg V, Jakopic G, Schaur A, Tribus M, Schmidmair D, Kaindl R (2017) Thermal expansion, mechanical and optical properties of gallium and aluminum substituted Zn_2TiO_4 spinels. Mater Res Bull 95:367–379
8. Girish KM, Prashantha SC, Nagabhushana H (2017) Facile combustion based engineering of novel white light emitting Zn_2TiO_4:Dy^{3+} nanophosphors for display and forensic applications. J Sci Adv Mat Dev 2:360–370
9. Chaves AC, Lima SJG, Araújo RCMU (2006) Photoluminescence in disordered Zn_2TiO_4. J Solid State Chem 179:985–992
10. Marin SJ, O'Keeffe M, Partin DE (1994) Structure and Crystal chemistry of ordered spinels: $LiFe_5O_8$, $LiZnNbO_4$ and Zn_2TiO_4. J Solid State Chem 113:413–419
11. Tanabe Y, Sugano S (1954) On the absorption spectra of complex ions I. J Phys Soc Jpn 9:753–766
12. Tanabe Y, Sugano S (1954) On the absorption spectra of complex ions II. J Phys Soc Jpn 9:766–779
13. Tanabe Y, Sugano S (1956) On the absorption spectra of complex ions III, the calculation of the crystalline field strength. J Phys Soc Jpn 11:864–877
14. Markevich I, Stara T, Khomenkova L, Kushnirenko V, Borkovska L (2016) Photoluminescence engineering in polycrystalline ZnO and ZnO-based compounds. AIMS Mater Sci 3:508–524
15. Sosman LP, López A, Câmara AR, Pedro SS, Carvalho ICS, Cella N (2017) Optical and structural properties of Zn_2TiO_4:Mn^{2+}. J Electron Mater 46:6848–6855
16. Espinoza VAA, López A, Neumann R, Sosman LP, Pedro SS (2017) Photoluminescence of divalent cobalt ions in tetrahedral sites of zinc orthotitanate. J Alloy Compd 720:417–422
17. Lokesh B, Rao NM (2016) Effect of Cu-doping on structural, optical and photoluminescence properties of zinc titanates synthesized by solid state reaction. J Mater Sci Mater Electron 27:4253–4258
18. Girish KM, Prashantha SC, Naik R, Nagabhushana H (2017) Zn_2TiO_4: a novel host lattice for Sm^{3+} doped reddish orange light emitting photoluminescent material for thermal and fingerprint sensor. Opt Mater 73:197–205
19. Roisnel T, Rodriguez-Carvajal J (2010) Fullprof suite program Fullprof 2 k V 480 Laboratoire Leon Brillouin (CEA-CNRS). https://www.ill.eu/sites/fullprof/. Accessed 15 Feb 2019
20. Millard RL, Peterson RC, Hunter BK (1995) Study of the cubic to tetragonal in Mg_2TiO_4 and Zn_2TiO_4:Mn^{2+} spinels by ^{17}O MAS NMR and Rietveld refinement of X-ray diffraction data. Am Mineral 80:885–896
21. Shannon RD (1976) Revised effective ionic radii and systematic studies of interatomic distances in halides and chalcogenides. Acta Crystallogr A 32:751–767
22. Basaravaju N, Sharma S, Bessiere A, Viana B, Gourier D, Priolkar KR (2013) Red persistent luminescence in $MgGa_2O_4$:Cr^{3+}; a new phosphor for in vivo imaging. J Phys D 46:375401
23. Liu C, Xia Z, Moolekev MS, Liu Q (2015) Synthesis, crystal structure, and enhanced luminescence of garnet-type $Ca_3Ga_2Ge_3O_{12}$:Cr^{3+} by codoping Bi^{3+}. J Am Ceram Soc 98:1870–1876
24. Jia-Chi Z, Qing-Song Q, Ming-Hui Y, Hong-Liang Z, Mei-Jiao Z (2011) Photoluminescence and persistent luminescence properties of non-doped and Ti^{4+} -doped Mg_2SnO_4 phosphors. Chin Phys B 9:094211
25. Henderson B, Imbusch GF (1989) Optical spectroscopy of inorganic solids. Oxford University Press, Oxford
26. Henderson B, Bartram RH (2000) Crystal-field engineering of solid-state laser materials. Cambridge University Press, Cambridge
27. Duan X, Liu J, Wu Y, Yu F, Wan X (2014) Structure and luminescent properties of Co^{2+}/Cr^{3+} co-doped $ZnGa_2O_4$ nanoparticles. J Lum 153:361–368